CHAPTER 2 THEORY AND LITERATURE REVIEW

2.1 Introduction

This research project was focused on the synthesis of dinuclear ionic copper(II) mixed carboxylates of general formula, $K_n[Cu_2(p\text{-}OC_6H_4COO)_n(RCOO)_{4-n}]$, where n = 1-3, and R is $CH_3CH{=}CH$- (2-butenoate), $CH_2{=}\underset{|}{C}\text{-}CH_3$ (2-methylpropenoate), $CH_3(CH_2)_7CH{=}CH(CH_2)_7$- (octadec-9-enoate), $(CH_3)_3C$- (2,2-dimethylpropanoate), $CH_3(CH_2)_3\underset{|}{C}H(C_2H_5)$ (2-ethylhexanoate) and $CH_3(CH_2)_7\underset{|}{C}H(CH_2)_5CH_3$ (2-hexyldecanoate). These complexes were specially designed to be low-temperature and thermally stable magnetic and redox-active materials. Then, suitably colored complexes are further analysed for their potential use as solar cell materials by photoluminescence spectroscopy.

As such, this chapter presents the general chemistry of copper(II) carboxylates, followed by the basic concepts used for the elucidation of their structures, namely elemental analyses, FTIR spectroscopy and UV-vis spectroscopy, and finally on magnetism, thermogravimetry, differential scanning calorimetry, cyclic voltammetry and photoluminescence spectroscopy.

2.2 Copper(II) Carboxylates

Copper(II) carboxylates ($[Cu_2(RCOO)_4]$, where R may be an alkyl or aryl group) are low-dimensional and thermally stable dinuclear complexes. They are easily prepared from cheap non-poisonous starting materials, namely copper(II) salts (chloride, nitrate, sulphate, acetate) and alkyl or arylcarboxylic acids.

2.2.1 Structural elucidation

Copper(II) carboxylates were reported to mainly adopt the paddle-wheel structure (**Figure 2.1**), which is similar to the structures of other metal(II) carboxylates [1].

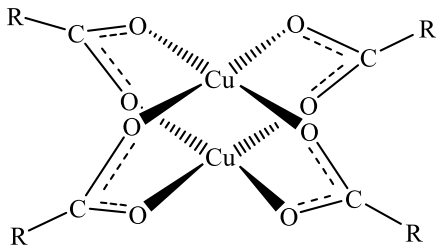

Figure 2.1 The paddle-wheel structure of $[Cu_2(RCOO)_4]$

In the above structure, $RCOO^-$ anion is shown as a bridging bidentate ligand. However, the anion is actually a versatile ligand, and has been known to show three main coordination modes with metal ions: *syn-syn, syn-anti,* and *anti-anti* (**Figure 2.2**).

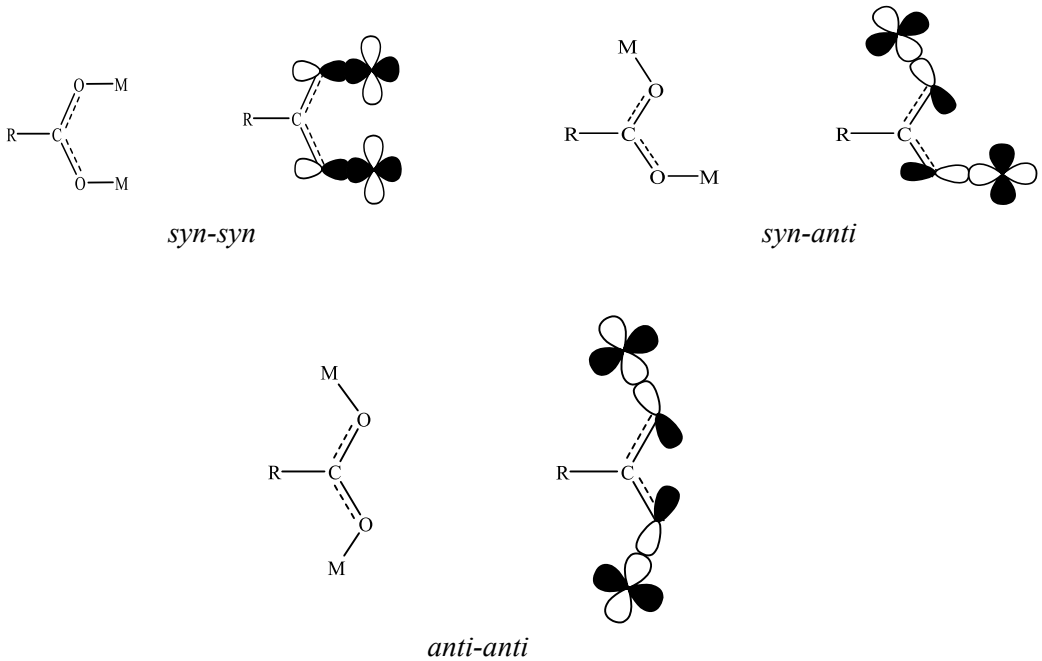

Figure 2.2 Coordination modes of $RCOO^-$ anion

In the paddle-wheel structure (*syn-syn* coordination mode for $RCOO^-$), only one of the lone pairs of its oxygen atom is used to form a coordinate covalent bond with a Cu(II) ion. As such, the second lone pair may be used to form a coordinate bond to a Cu(II) centre of another paddle-wheel unit, to form a polymeric structure (**Figure 2.3**) [1]. The coordinate bonds linking the dimers are weak and result in a crankshaft appearance of the column [2].

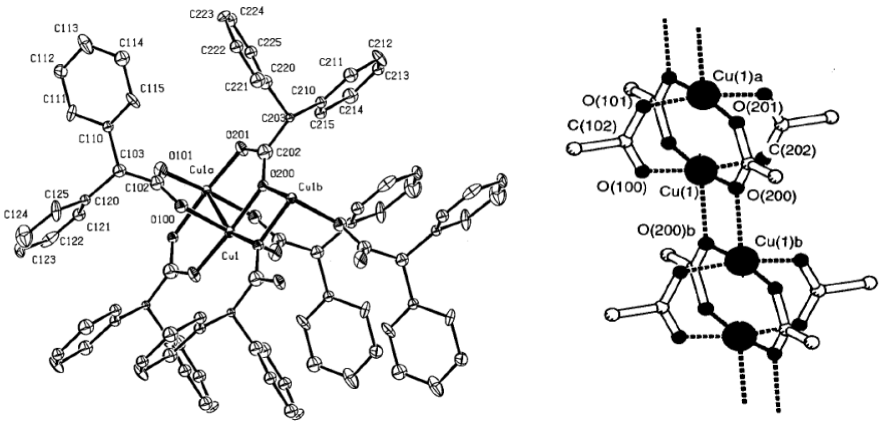

(a) (b)

Figure 2.3 Structure of (a) bis(μ-diphenylacetato-*O*:*O*')dicopper(II); and (b) *catena*-poly[[bis(μ-diphenylacetato-*O*:*O*')dicopper](μ_3-diphenylacetato-1-*O*:2-*O*':1'-*O*')(μ_3-diphenylacetato-1-*O*:2-*O*':2'-*O*')] (showing only the linkage at the centres)

The dinuclear paddle-wheel structure may also be linked to form polymeric structures by neutral ligands, such as ethanol, pyrazine, 2-aminopyrimidine and dioxane. An example is shown in **Figure 2.4** [1].

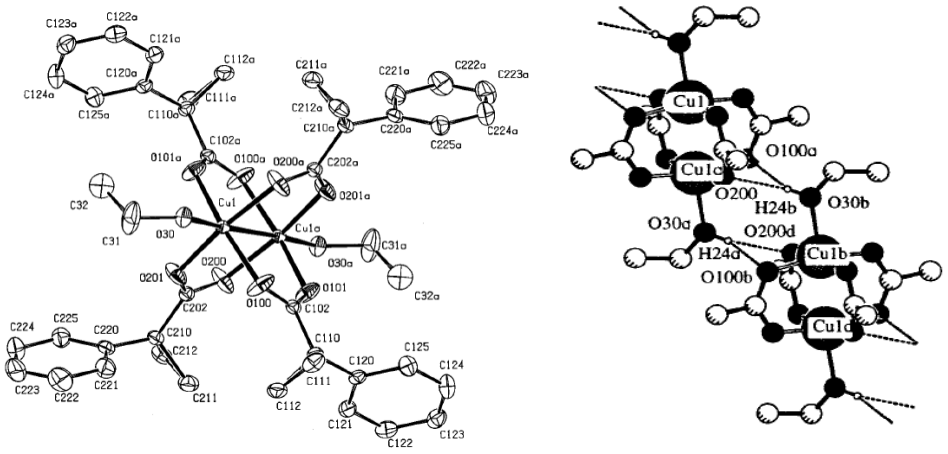

(a) (b)

Figure 2.4 Structure of (a) tetrakis(μ-1-phenylcyclopropane-1-carboxylato-*O*,*O*')bis(ethanol-*O*)dicopper(II); and (b) poly[tetrakis(μ-1-phenylcyclopropane-1-carboxylato-*O*,*O*')bis(ethanol-*O*)dicopper(II)] (showing only the linkage at the centres)

(a) Elemental analyses

Elemental analyses is a quick method to determine the percentage of an element in a compound such as carbon (C), hydrogen (H) and nitrogen (N), and hence the empirical formula of the compound. An empirical formula shows the smallest integer ratio for the elements that gives the correct elemental composition by mass. The composition of a compound is often expressed in terms of the weight percent for each element in the compound. The analyzer uses excess oxygen to completely combusted an element in the compound to simple gases. For example, C, H and N are converted to CO_2, H_2O, and N_2 respectively. A typical equation is:

$$C_xH_yA + z\ O_2\ (g) \rightarrow x\ CO_2\ (g) + y/2\ H_2O\ (g) + A$$

In the above equation, the symbol A represents elements other than C and H which burn to produce either a solid residue or gas. The gaseous products are separated under steady state conditions, and measured as a function of thermal conductivity.

In the analyses, the impurities introduced by the equipment, such as the furnace, crucible, detectors, and the inert gas (helium), have to be taken into consideration. To compensate the effect of these impurities, a series of tests could be run with and without the sample, and to achieve accurate measurements, there should be complete combustion of the sample.

(b) Fourier transform infrared spectroscopy

Fourier transform infrared spectroscopy (FTIR) involves infrared radiation between the visible and microwave regions, and normally 4000 cm^{-1} – 400 cm^{-1} [3]. This amount of energy is sufficient to cause changes in the vibrational energy levels of a molecule.

An FTIR spectrum shows peaks that correspond to the frequencies of vibrations (normally in wavenumber, cm^{-1}) between covalently bonded atoms (types of chemical bonds and functional groups). Thus, different molecular structures produce different spectra (just like fingerprints). Hence, this technique is useful at it can be used to identify unknown materials. It is also a non-destructive technique, fast and providing precise measurement which requires no external calibration.

For metal carboxylates, an FTIR spectrum may be used to deduce the binding mode of the carboxylate ligands (RCOO). This is based on the difference (ΔCOO) between the values of $\upsilon_{asym}COO$ (normally at about 1550 cm^{-1}) and $\upsilon_{sym}COO$ (normally at about 1390 cm^{-1}). There are three main binding modes: monodentate, bridging and chelating. The ΔCOO value of larger than 200 cm^{-1} indicates monodentate coordination [4], values in the range of 130-180 cm^{-1} indicate bridging coordination [1,5], while values lower than 120 cm^{-1} indicate chelating coordination.

(c) UV-visible spectroscopy

UV-visible spectroscopy (UV-vis) covers the electromagnetic region between 200 nm (high energy) to 1000 nm (low energy). The energy within this region provides sufficient energy to cause electronic transitions in a molecule. This spectroscopic technique may be used in quantitative and qualitative analyses, and it can be done for solid and liquid samples.

For a quantitative analysis, the equation used is known as the Beer-Lambert's law: $A = \varepsilon cl$, where A is the absorbance (no unit), ε is the molar absorptivity ($dm^3\ mol^{-1}\ cm^{-1}$), c is the molarity of the solution ($mol\ dm^{-3}$), and l is the path length of the light (cm).

Most transition metal complexes are colored due to an excitation of an electron from one *d* orbital of lower energy to another *d* orbital of higher energy (*d-d* electronic transition). This occurs as a result of absorption of energy corresponding to the visible region of the electromagnetic radiation. The colour and the energy absorbed may be deduced from the colour wheel (**Figure 2.5**). For example, the spectrum of a green sample will have absorption peaks within 620-800 nm, which is in the red region (red is the complementary colour to green).

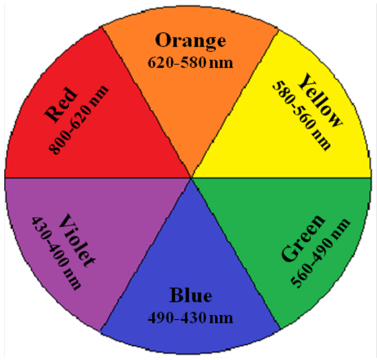

Figure 2.5 Colour wheel

There are two types of electronic transitions for transition metal complexes: charge transfer (CT) and *d-d* transitions. The ligand-metal charge transfer (LMCT)

refers to an electronic excitation from the orbitals of the ligand ("oxidation") to those of the metal ("reduction"). The opposite applies for metal-ligand charge transfer (MLCT). The CT bands are normally in the UV region (high energy), and highly intense ($\varepsilon > 10^3$ dm^3 mol^{-1} cm^{-1}).

The *d-d* transition refers to electronic excitation from a *d* orbital of lower energy to another *d* orbital of higher energy. These bands are normally in the visible region (lower energy). The intensity of the bands is much lower than the CT bands. According to La Porte rule, complexes with a centre of inversion (octahedral and square planar), the *d-d* transition is forbidden transition (but multiplicity allowed). Thus, these complexes usually have pale colours and the spectrum shows a weak band ($\varepsilon \sim$ 1-10 dm^3 mol^{-1} cm^{-1}). On the other hand, complexes with no centre of inversion (tetrahedral, square pyramidal) are not governed by this rule, and therefore are more highly coloured and the spectrum shows a stronger band ($\varepsilon \sim 100$ dm^3 mol^{-1} cm^{-1}).

UV-vis spectra of copper(II) complexes are useful as they provide information on the geometry of copper(II) ion, deduced from the wavelength of the *d-d* band. For example, the band expected for a tetrahedral complex (**Figure 2.6(a)**) is normally at 800 nm, a square pyramidal complex (**Figure 2.6(b)**) is normally at 700 nm [6], and a square planar complex (**Figure 2.6(c)**) is normally at 600 nm [7].

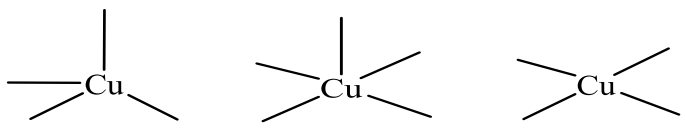

(a) (b) (c)

Figure 2.6 geometry at the copper center (a) tetrahedral; (b) square pyramidal; and (c) square planar

For dinuclear copper(II) carboxylates in the paddle-wheel structure, the geometry of the copper(II) centres are square planar. The *d-d* energy levels are split as shown in

Figure 2.7. Thus, their UV-vis spectra usually show two weak *d-d* bands. The band at a lower energy (termed Band I) is assigned to $d_{xz},d_{yz} \rightarrow d_{x^2-y^2}$ transition [8,5]. The second band (termed Band II) is normally observed as a shoulder to the lower energy side of a much stronger CT band (π-π^*) [9]. Band II arises from Cu(II)-Cu(II) interaction, thus indicating a dimeric complex [10,5].

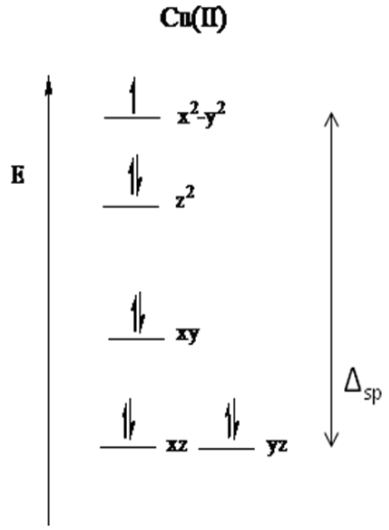

Figure 2.7 The energy of the *d* orbitals in a square planar copper(II) centre

2.2.2 Thermal properties

Two main techniques used to determine the thermal properties of a compound are thermogravimetry and differential scanning calorimetry.

(a) Thermogravimetry

Thermogravimetric analysis (TGA) measures the amount (normally as %) of weight loss of a sample as the temperature is increased (to about 1000^{o}C) in a controlled atmosphere (normally N_2). The weight loss is probably due to evaporation (loss of volatiles), decomposition (breaking of chemicals bonds), reduction (interaction of the sample in a reducing atmosphere), and/or desorption.

In a TGA thermogram, a single or more weight loss(es) may be shown. The weight loss is based on the derivative weight loss [11]. An example is the step-like thermogram of calcium oxalate ($CaC_2O_4.H_2O$) (**Figure 2.8; Scheme 2.1)** [12].

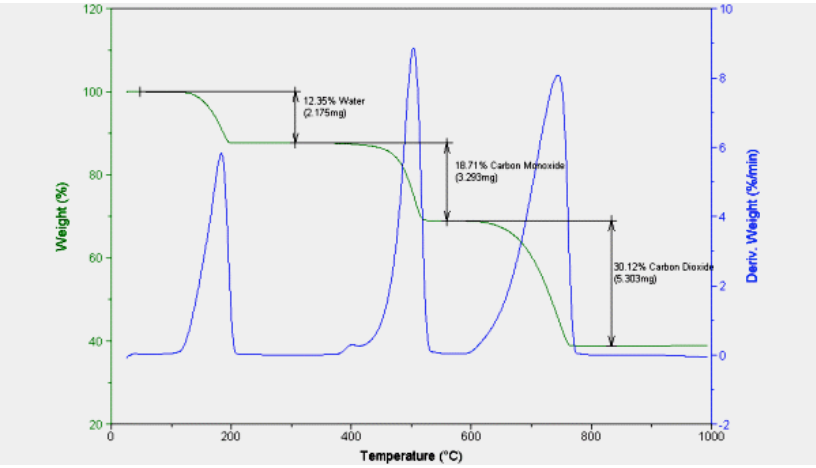

Figure 2.8 TGA of calcium oxalate ($CaC_2O_4.H_2O$)

$$CaC_2O_4.H_2O \xrightarrow{-H_2O} CaC_2O_4 \xrightarrow{CO} CaCo_3 \xrightarrow{-CO_2} CaO$$

Scheme 2.1 Thermal decomposition of $CaC_2O_4.H_2O$

A TGA thermogram indicates the temperature at which a sample is thermally stable. For example, **Figure 2.8** indicates that calcium oxalate is thermally stable up to 467^{o}C, above which the oxalate ligand decomposed to CO and CO_2. Most carboxylate ligands decomposed mainly by loss of CO_2 from the decarboxylation of the caboxylate ligands [13].

A TGA thermogram may also be used to estimate the formula mass of a metal complex from the residue formed (CuO) [13,10], and hence its chemical formula. Thus, this will further support the proposed structure in the absence of crystal data. The calculation is based on the gravimetric concept. However, this can only be done if the identity of the residue is known, and that the ligands are completely decomposed (as indicate by a plateau at high temperature) [13].

Copper(II) carboxylates are thermally stable as they do not decompose on heating at temperatures less than about 200°C. It is to be noted that copper(II) arylcarboxylates normally did not melt below the decomposition temperature. For example, $[Cu_2(C_6H_4CO_2)_4(EtOH)_2]$ (**Figure 2.9**) decomposed at 230°C (based on TGA) with no phase changes before that (based on DSC) [13].

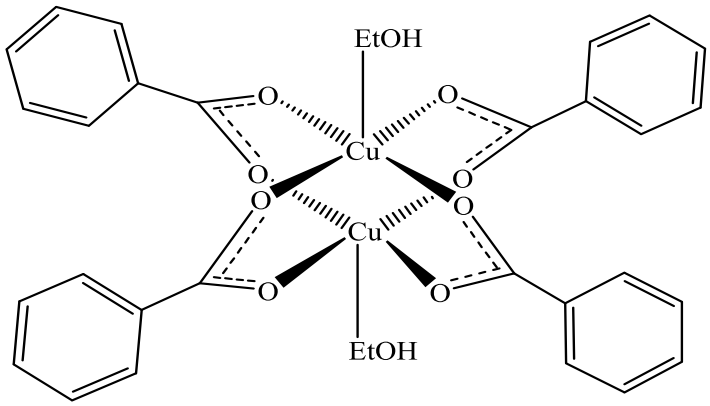

Figure 2.9 Structure of $[Cu_2(C_6H_4COO)_4(EtOH)_2]$

(b) Differential scanning calorimetry

Differential scanning calorimetry (DSC) is a technique to study the thermal transition of a sample. A thermal transition is defined as the transition from one phase to another as the heat is increased. DSC gives information of the molecule phase transition such as its glass transition temperature, melting temperature and clearing temperature [14]. DSC measures the difference in heat absorbed or released (ΔH) by a sample (**Figure 2.10**). The absorption of heat (endothermic process) can be ascribed to melting [15], glass transition [16] and chemical reaction [11]. On the other hand, releasing of heat (exothermic process) can be ascribed to crystallization and bond formation [15,16].

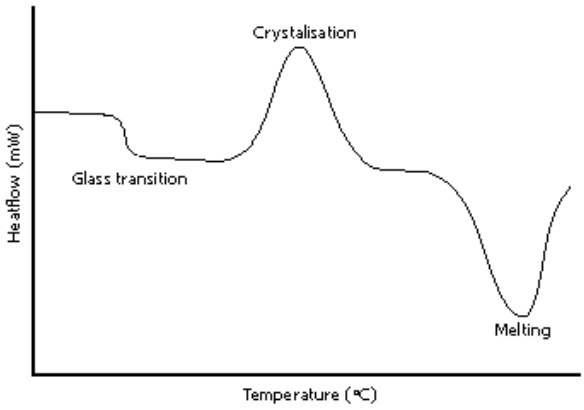

Figure 2.10 Features and assignation of DSC curve

Copper(II) alkylcarboxylates, especially for large alkyl group, have low melting points. For examples, the melting temperature for $[Cu_2(CH_3(CH_2)_{14}COO)_4]$ (**Figure 2.11**) is 112°C, while its clearing temperature is 220°C [2].

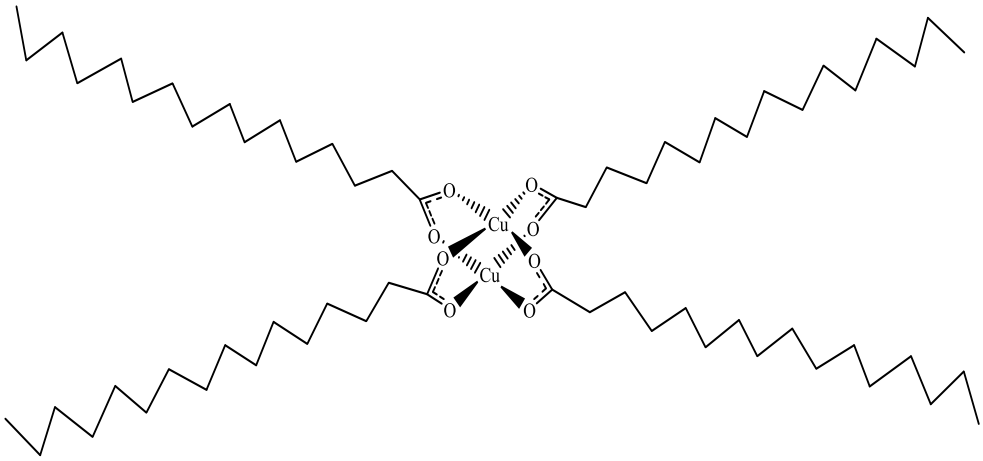

Figure 2.11 Structure of $[Cu_2(CH_3(CH_2)_{14}COO)_4]$

The melting temperatures of copper(II) complexes of linear alkylcarboxylates normally increase with increasing number of carbon atom. Examples are $[Cu_2(CH_3(CH_2)_8COO)_4]$ (m.p. 103°C), $[Cu_2(CH_3(CH_2)_9COO)_4]$ (m.p. 107°C) and $[Cu_2(CH_3(CH_2)_{16}COO)_4]$ (m.p. 116°C) [17].

The melting temperatures of copper(II) complexes of branched alkylcarboxylates are expectedly much lower than the linear analog. For example, the melting temperature of tetrakis(μ-(2,2-(dioctyl(acetate))-*O*,*O*')biscopper(II) (**Figure 2.12**) is -20^{o}C. However, it is interesting to note that this complex has similar decomposition temperature (T_{dec} = 214^{o}C [2] as other copper(II) carboxylates, suggesting no correlation between melting and decomposition temperatures.

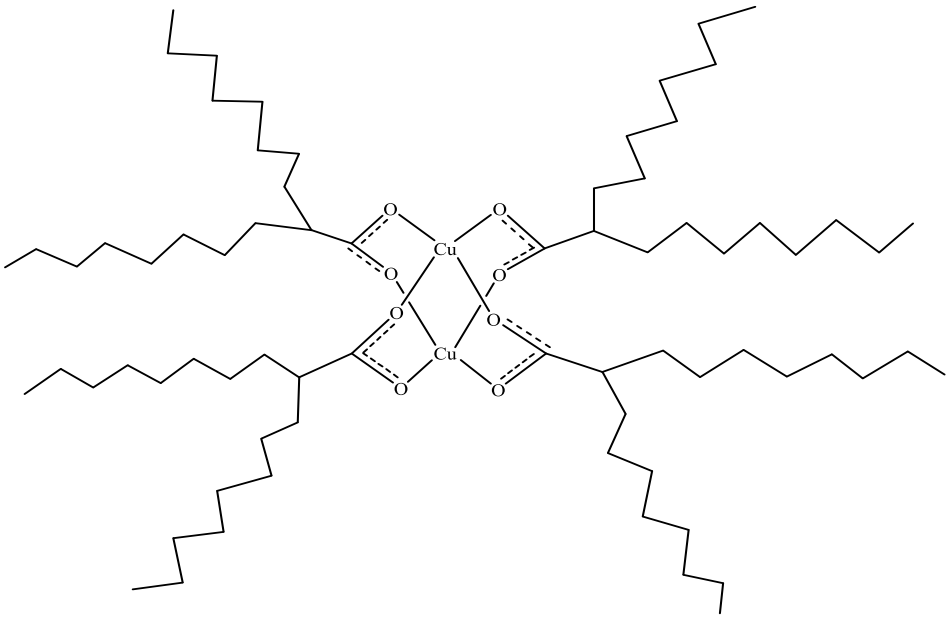

Figure 2.12 Structure of tetrakis(μ-(2,2-(dioctyl(acetate))-*O*,*O*')bis(copper(II)

Copper(II) complexes with unsaturated alkylcarboxylates also have low melting temperatures. For example, the melting temperature of $[Cu_2((CH_3)_2C{=}CH(CH_2)_2(CH_3)CHCH_2COO)_4]$, $[Cu_2(CH_2{=}CH(CH_2)_8COO)_4]$ and $[Cu_2(CH_3(CH_2)_7CH{=}CH(CH_2)_7COO)_4]$ is 70^{o}C, 44^{o}C and 33^{o}C respectively, [17].

2.2.3 Magnetism

Magnetism is defined as a force of attraction or repulsion that responds at an atomic or subatomic level to an applied magnetic field. This is due to a magnetic field caused by

moving electrically charged particles. The attraction toward a magnetic field is termed paramagnetic, while repulsion out of a magnetic field is termed diamagnetic.

Paramagnetism arises from the presence of unpaired electron(s), which are randomly aligned in the absence of an applied magnetic field (**Figure 2.13(a)**). In contrast, diamagnetism arises from paired electrons, thus no net magnetic moments (**Figure 2.13(b)**).

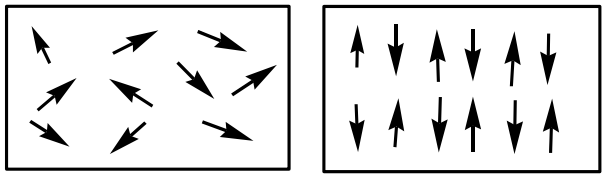

Figure 2.13 Alignment of electrons in a sample: **(a)** paramagnetic; **(b)** diamagnetic

In the bulk magnetic properties, there are three types of paramagnetism: antiferromagnetism, ferromagnetism and ferrimagnetism. In antiferromagnetic materials, the unpaired electron(s) is/are aligned in a regular pattern and the directions of neighbouring spins are anti-parallel (**Figure 2.14(a)**). In ferromagnetic materials, the unpaired electrons are aligned in the same direction in the absence of an external magnetic field (**Figure 2.14(b)**). Thus, a ferromagnetic substance forms a strong and permanent magnet. In ferrimagnetic materials, the unpaired electrons are in a parallel alignment but with different strength of magnetic spin (**Figure 2.14(c)**) [18, 19].

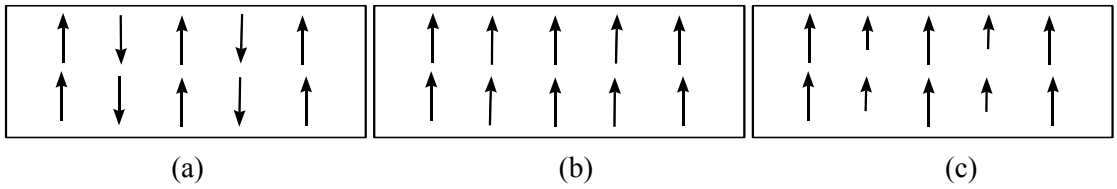

Figure 2.14 Electron alignment in a paramagnetic sample: (**a**) antiferromagnetism; (**b**) ferromagnetism; (**c**) ferrimagnetism

Magnetic properties of a material may be deduced from the value of its effective magnetic moment, μ_{eff}. This is calculated from the experimental data using the following equations:

$$\chi_M = \chi_g \times M_r$$

$$\chi_M^{corr} = \chi_M - \chi_D$$

$$\mu_{eff} = 2.828(\chi_M^{corr} T)^{½}$$

where χ_M is molar magnetic susceptibility, χ_g is gram magnetic susceptibility (reading from the instrument), M_r is the formula mass, χ_D is the magnetic susceptibility corrected from the diamagnetic contributions of all the atoms in the molecule (refer to Pascal Table), χ_M^{corr} is the corrected molar magnetic susceptibility, and T is the absolute temperature.

Copper(II) ion (valence electronic configuration: $3d^9$) has one unpaired electron. The theoretical μ_{eff} value for mononuclear copper(II) complexes, calculated using the spin-only equation: $\mu_{eff} = [n(n+2)]^{½}$ (where n is the number of unpaired electron), is 1.73 B.M., while that for dimeric copper(II) carboxylates (two unpaired electrons), the value is 2.83 B.M.

However, many copper(II) carboxylates exhibit sub-normal magnetic moments. For examples, the magnetic moment for $[Cu_2(CH_3COO)_4(H_2O)_2]$ (**Figure 2.15**) was found to be 1.43 B.M. (calculated per Cu) [19]. This is due to an antiferromagnetic interaction between the two copper(II) centres, postulated to occur through the bridging carboxylate ligands, termed the superexchange pathway [20].

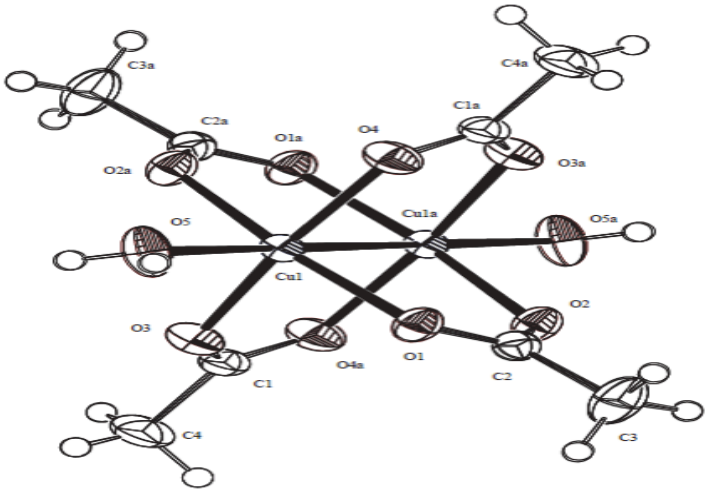

Figure 2.15 Structure of $[Cu_2(CH_3COO)_4(H_2O)_2]$

The magnitude of the magnetic interaction may be inferred from the value of 2J, which is a measure of the separation energy of the singlet ground state and triplet excited state. For a dimeric copper(II) complex, the 2J value is calculated using the Bleaney-Bowers equation:

$$\chi_m = 2Ng^2\beta^2/(3kT)*\{1+1/3\exp(-2J/kT)\}^{-1} + 0.12x10^{-3}$$

A negative 2J value indicates antiferromagnetic interaction (singlet ground state), while a positive value indicates a ferromagnetic interaction (triplet ground state). Generally, the 2J values for dinuclear Cu(II) carboxylates were observed in the range of -280 cm^{-1} to -330 cm^{-1} [21]. For example, the 2J value for a dimeric Cu(II) acetate with water molecules as the axial ligands (**Figure 2.15**) is -292.2 cm^{-1} [22].

The 2J values are affected by the nature of the ligand attached at the axial positions of the Cu(II) centres. For example, the 2J value was found to be more negative (stronger antiferromagnetic interaction) when the axial ligands are weaker bases (weaker σ donation of the axial ligand) [20, 23].

2.2.4 Redox properties

Cyclic voltammetry (CV) is an electrochemical technique used to probe the redox properties of a material. This technique involves changes in the potential of the working electrode (WE) with respect to the reference electrode (RE) at a constant rate, while measuring the current. Hence a plot of current *vs*. potential (or a voltamogram) is produced.

A redox reaction describes a chemical reaction of an atom, which can be either oxidation or reduction. Oxidation is an increase in the oxidation state or loss of electron(s). On the other hand, reduction is a decrease in oxidation state or gain of electron(s).

The electrodes that may use in a cyclic voltammetric determination are glassy carbon as a working electrode, saturated calomel electrode as a reference electrode and platinum wire as a counter electrode. The electrolyte may be tetrabutylammonium tetrafluoroborate.

Three types of electron transfer are possible: reversible, quasireversible and irreversible. Reversible electron transfer occurs when there is an equilibrium mixture of products and reactants. Reversibility is associated with a fast electron transfer and slow mass transport. The criteria of reversible process is shown in the **Figure 2.16**, where the values of the peak separation, $\Delta E_p = E_{pa} - E_{pc} = 59$ mV (assuming one-electron process) and $I_{pc}/I_{pa} = 1$ [23]. Thus, the most important parameters in CV are the anodic peak potential (E_{pa}) and cathodic peak potential (E_{pc}), cathodic peak current (I_{pc}), and anodic peak current (I_{pa}).

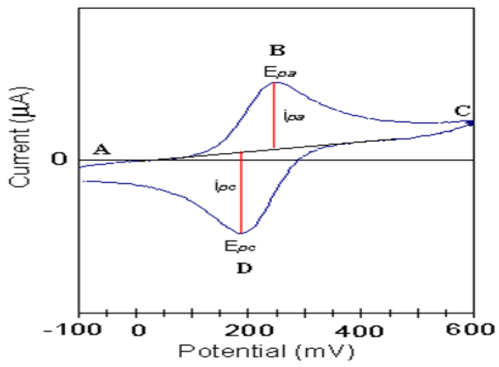

Figure 2.16 Cyclic voltammogram of a reversible process

Quasireversible electron transfer arises from a slow electron transfer from the product back to the initial state. The ΔE_p value for this process is greater than 59 mV. Most dimeric copper(II) carboxylates undergo quasireversible redox process (ΔE_p= ~150 - 280 mV) involving more than one-step [13].

For a irreversible redox process, the change in thermodynamic state from the product to the reactant cannot be precisely restored. To determine an irreversible process, the voltamomgram usually show only one peak (whether oxidation or reduction). Sometimes the irreversibility behavior occurs when there is a destructive process of a species, which then lead to the formation of a more stable geometry. Some dimeric copper(II) carboxylates have been reported to have irreversible redox properties [24].

2.3 Solar Materials

The current energy crisis arises from the depletion of the main energy resources, the fossil fuels. It is a challenge to find a new source of clean sustainable energy, such as solar, wind and hydroelectric energy.

Earth receives abundant and clean energy from the sun. Hence, solar energy is ideal as an alternative energy source to fossil fuels. Solar energy can be converted to

either heat energy or electricity. There are two ways to convert the rays from the sun to electricity: photovoltaic cells (PV) and solar power plant. PV changes the sunlight directly into electricity, while solar power plant indirectly generates electricity when the heat from a solar thermal collector is used to heat a fluid, which then produces steam that is used to power the generator [25].

Coordination metal complexes with conjugated polymers as ligands are potential solar materials [26]. This is because the metal ions may act as the templates to assemble the organic subunits, and are redox-active and paramagnetic to generate active site for charge transport which may alter the electrochemical and optical energy of the π-systems. Additionally, their HOMO-LUMO gaps may be easily tuned through interaction of the *d*-orbitals with the ligand orbitals. Diversity of molecular frameworks can be observed among different metals based on their different coordination number, geometry and valence shells [27]. Examples are platinum(II) arylene ethynylenes. In these complexes, the *d* orbitals of platinum(II) overlap with the *p* orbitals of the alkyne unit, which leads to an enhancement of π-electron delocalization and to intrachain change transport.

Intersystem crossing is enhanced by spin-orbit coupling. This allows for the formation of triplet excitons, and thus extended exciton diffusion lengths [26-29].

The photochemistry of copper complexes had been studied. Copper complexes may show several redox reactions in the excited state, such as ligand-to-metal charge-transfer (LMCT), metal-to-ligand charge-transfer (MLCT), charge-transfer-to-solvent (CTTS), intraligand (IL), interconfigurational metal-centered (IMCT) and ligand-to-ligand charge-transfer (LLCT) [30-31].

2.3.1 Band gap

Band gap (E_g) is defined as the difference of energy between the top of the valence band and the bottom of the conduction band (**Figure 2.17**). The band gap measurement is important in solar industries, semiconductors and nanomaterials.

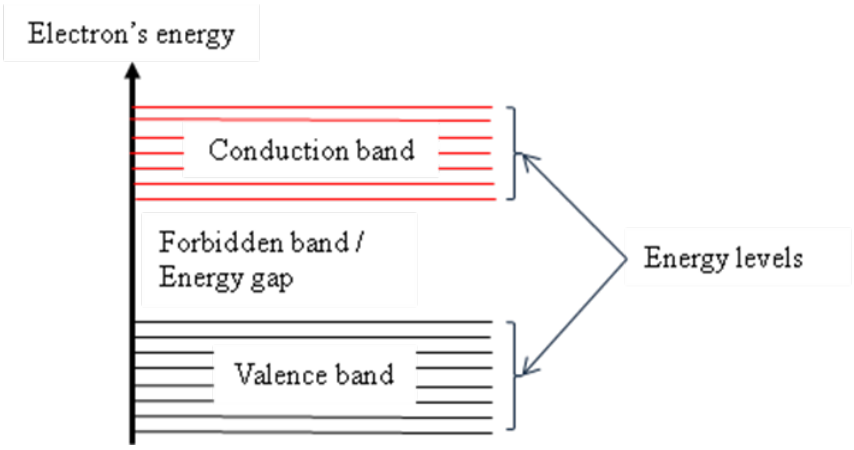

Figure 2.17 Energy arrangement in atoms

Electrons in the upper band are easily removed by the application of external electric fields. This band is termed the conduction band. A good conductor has a large number of electrons in the conduction band. In the middle lies the forbidden band or energy gap. There are no electrons in this band. Thus, the electrons may travel back and forth but they do not rest in this band. Hence, the band gap energy is the minimum energy for the transition. The valence bands have series of energy level containing valence electrons. In order to move the electrons from the valence band to the conduction band, energy such as thermal energy is required. This is because electrons in the valence band are bonded to the individual atom.

The width of the forbidden band can determine whether a material is an insulator, semiconductor or conductor. An insulator shows very broad energy gap ($E_g > 4$ eV). For

a semiconductor, the value of E_g is less than 3 eV, while there is no energy gap in a conductor (the valence and conduction bands overlap).

Experimentally, the band gap may be deduced by UV-vis spectroscopy (the optical band gap) and cyclic voltammetry (the electrochemical band gap). The optical band gap is calculated from the equation: $E_g = hc/(\lambda \times 1.6\text{x}10^{-19})$ eV, where h is Planck constant (6.626×10^{-34} J s); c is the speed of light (3.0×10^8 m s^{-1}) and λ was the onset wavelength that corresponds to the CT band from the UV-vis spectrum.

The electrochemical energy gap is calculated using the equation: $E_g = \Phi'_p - \Phi'_n$. It is the difference between energy of the lowest unoccupied molecular orbital (LUMO; Φ'_p) and the highest occupied molecular orbital (HOMO; Φ'_n). The onset potential of reduction and oxidation processes are determined from the voltammogram. The LUMO and HOMO energy levels are E_{LUMO} and E_{HOMO} adding with 4.4 V to each of the potentials, respectively [32].

Various forms of TiO_2 were also studied as solar materials. Unfortunately, the band gaps of these semiconductors are wide (3.30-3.87 eV) [33, 34].

Photovoltaic properties of metal complexes normally studied are based on platinum (Pt), cadmium (Cd), lead (Pb), indium (In) and tellurium (Te). An example is Pt-phenylene polyyne. However, the optical E_g of this complex is large (~3.0 eV) [27, 35]. Additionally, there are serious concerns with the use of these metal complexes: cadmium and lead are heavy metal with high toxicity, while indium and tellurium are the least abundant elements [36]. Thus, several researches seek alternative metals as solar cell materials. Examples are titanium (Ti) and copper (Cu).

In order to tune for a lower energy-gap, the chromophores features may undergone intramolecular charge transfer (ICT) and increased the number of electron withdrawing group. This is because it enhance the electron-accepting properties [27].

Based on the availability and cost, copper is a suitable alternative solar material [37]. The bang gap value for copper(I) oxide (Cu_2O) and copper(II) oxide (CuO) are 1.4 eV and 2.0 eV respectively [38,39]. Copper(I) sulfide (Cu_2S) also has a lower band gap energy value of 2.0 eV [40]. These show that copper compounds may acts as a *p*-type semiconducting materials.

2.3.2 Photoluminescence spectroscopy

Photoluminescence spectroscopy is widely used to measure the emission of light from various types of samples (gases, liquids and solids) after they are excited by light. This occurs when a photon excites an electron from the ground state to an excited state. Light is emitted when the excited electron returns back to the ground state. The electron transfer process is the key step for an artificial photosynthesis as well as in natural photosynthesis.

The process of absorption and emission is described by the Jablonski diagram (**Figure 2.18**). Fluorescence occurs at a lower energy since the energy of emission is less than that of absorption [41].

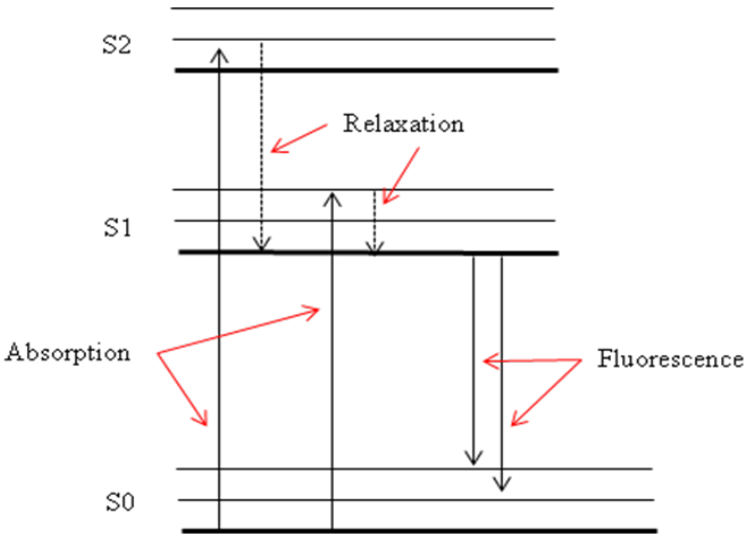

Figure 2.18 Jablonski diagram

Based on the paper reported by Ressalan *et al*. [42], a quenching effect occurs due to complexation of a ligand and a copper(II) ion. This happens when there is an interaction between the excited ligand and the non-excited copper(II) ion. This occurs when the energy of the *d* orbitals of copper complexes was split by the ligand field then combines with the ligand orbitals and produces additional states. The excitation energy is transferred from the ligand π* orbital to copper(II) *d*π orbital by energy transfer and electron transfer process.

References

[1] F. P. W. Agterberg, H. A. J. P. Kluit, W. L. Drissen, H. Oevering, W. Buijs, M. T. Lakin, A. L. Spek and J. Reedijk, *Inorg. Chem.*, 36 (1997) 4321

[2] G. S. Attard, P. R. Cullum. *Liq. Cryst*., 8(3), (1990) 299

[3] R. M. Silverstein, and F. X. Webster, *6th edn. New York: John Wiley & Sons* (1998). Spectrometric Identification of Organic Compounds

[4] Á. García-Raso, J. J. Fiol, A. López-Zafra, J. A. Castro, A. Cabrero, I. M. E. Molins, *Polyhedron*, 22, (2003) 403

[5] M. Pajtášová, D. Ondrušová, E. Jóna, S. C. Mojumdar, S. L'alíková, T. Bazyláková, M. Gregor, *J. Therm. Anal. Calorim*. 100 (2010) 769

[6] Y.Y.Wang, Q.Shi, Q.Z.Shi, Y.C.Gao, X.Hou, *Polyhedron*, 19 (2000) 891

[7] K.S.Bharati, S.Sreedaran, A.K. Rahiman, K.Rajesh, V.Narayanan, *Polyhedron,* 26 (2007) 3993

[8] X. Zhuang, T. Lu and S. Chen, *Inorganica Chimica Acta*, 358 (2005) 2129

[9] A. Ray, D. Sadhukhan, G. M. Rosair, C. J. Gómez-García and S. Mitra, *polyhedron* 28 (2009) 3542

[10] M. A. Agotegaray, M. A. Boeris and O. V. Quinzani, *Sociedade Brasileira de Químic,* 21(12), (2010) 2294

[11] F. Rodriguez, (1996). *Principles of Polymer System*, 4th edn. Washington: Taylor & Francis

[12] H. Chang and P. J. Huang, *Anal Chem*. 69 (1997) 1485

[13] M. I. Mohamadin and N. Abdullah, *Cent. Eur. J. Chem*. 8 (2010) 1090

[14] L. Y. Park and J. M. Rowe, *Chem. Mater*. 10 (1998) 1069

[15] H-G. Elias, *Macromolecules: Structure and Properties.* (1984). New York: Plenum Press

[16] P. Maldivi, L. Bonnet, A-M. Giroud-Godquin, M. Ibn-Elhaj, D. Guillon and A. Skoulios, *Adv. Mater.*, 5, (1993) 909

[17] G. I. Likthenshtein, J. Yamauchi, S. Nakatsuji, A. I. Smirnov, and R. Tamura, *Nitroxides: Applications in Chemistry, Biomedicine, and Materials Science*, WILEY-VCH Verlag GmbH & Co. KGaA, Weinheim, chapter 1, 2008,

[18] D. F. Shriver, P. W. Atkins, *Inorganic Chemistry*, Oxford University Press 4rd ed., Page. 600.

[19] M. Kato, H. B. Jonassen and J. C. Fanning, *Chem. Rev*. 64 (1964) 99

[20] M. Melnik, *Coord. Chem. Rev.,* 42 (1982), 259

[21] A. Emali, *Turk. J. Phy.*, 24 (2000) 667

[22] M. Kato and Y. Muto, *Coord. Chem. Rev*. 92 (1988) 45

[23] http://en.wikipedia.org/wiki/Cyclic_voltamettry, (12 Feb 2010)

[24] I. Toledo, M. Arancibia, C. Andrade and I. Crivelli, *Polyhedron*, 17 (1998) 173

[25] http://205.254.135.24/kids/energy.cfm?page=solar_home-basics, (16 June 2011)

[26] W. –Y. Wong, C. –L. Ho, *Coord. Chem. Rev.* 250, (2006) 2627

[27] W. –Y. Wong, C. –L. Ho, *Accounts of Chemical Research*. 43, (2010) 1246

[28] G. R. Whittel, I. Manners, *Adv Mater*. 19, (2007) 3439

[29] T. L. Schull, J. G. Kushmerick, C. H. Patterson, C. George, M. H. Moore, S. K. Pollack, R. Shashidhar, *J. Am. Chem. Soc*. 125, (2003) 3202

[30] C. Kutal, *Coord. Chem. Rev*., 399 (1990) 213

[31] J. Sýkora, *Coord. Chem. Rev*., 159 (1997) 98

[32] D.M. de Leeuw, M.M.J Simenon, A.R. Brown and R.E.F Einerhand, *Synth. Met*. 87 (1997) 53.

[33] Z. Jiang, F. Yang, N. Luo, B. T. T Chu, P. Sun, H. Shi, T. Xiao, P. P. Edwards, *Chem. Commun*. (2008), 6732

[34] D. V. Bavykin, S. N. Gordeev, A. V. Muskalenko, A. A. Lapkin, F. C. Walsh, *J. Phys. Chem*., 109 (2005) 8565

[35] A. Köhler, H. F. Wittman, R. H. Friend, M. S. Khan, J. Lewis, J. *Synth. Meth.* 67 (1994) 245

[36] R. Debnath, J. Tang, D. A. Barkhouse, X. Wang, A. G. Pattentyus-Abraham, L. Brzozowski, L. Levina and E. H. Sargent, *Journal of American Chemical Society*, 132, (2010) 5952

[37] C. Wadia, A. P. ALivisatos, and D. M. Kammen, *Environmental Science & Technology*, 43, (2009) 2072

[38] F. P. Koffyberg and F. A. Benko, *Journal of Applied Physics*, 53, (1982) 1173

[39] G. Nagasubramanian, A. S. Gioda, and A. J. Bard, *Journal of Electrochemical Society*, 128, (1981) 2158

[40] C. Ratanatawanate, A. Bui, K. Vu, and K. J. Balkus, Jr, *J. Phys. Chem.*, 115 (2011) 6175

[41] E. Moreno-Garcia, C. E. Guerra-, J. M de la Rosa-Vázquez, *18th International Conferemce on Electronics, Communications and Computers*, (2008) 99

[42] S. Ressalan and C. S. P. Iyer, *Journal of Luminescence*, 111 (2005) 121